

1 **Temporal variability and driving factors of the carbonate system in the Aransas**

2 **Ship Channel, TX, USA: A time-series study**

3

4 **Melissa R. McCutcheon¹, Hongming Yao^{1,2}, Cory J. Staryk¹, Xinpeng Hu¹**

5 ¹ Harte Research Institute for Gulf of Mexico Studies, Texas A&M University – Corpus
6 Christi, TX 78412, USA

7 [#] current address: Shenzhen Engineering Laboratory of Ocean Environmental Big Data
8 Analysis and Application, Shenzhen Institute of Advanced Technology, Chinese
9 Academy of Sciences, Shenzhen 518055, China

10

11

12 *Correspondence to:* Melissa R. McCutcheon (melissa.mccutcheon@tamu.edu)

13

14

15 **Keywords:** *p*CO₂, acidification, diel variability, seasonal variability, autonomous sensors

16 **Abstract**

17 The coastal ocean is affected by an array of co-occurring biogeochemical and
18 anthropogenic processes, resulting in substantial heterogeneity in water chemistry,
19 including carbonate chemistry parameters such as pH and partial pressure of CO₂ (*p*CO₂).
20 To better understand coastal and estuarine acidification and air-sea CO₂ fluxes, it is
21 important to study baseline variability and driving factors of carbonate chemistry. Using
22 both discrete bottle sample collection (2014-2020) and hourly sensor measurements
23 (2016-2017), we explored temporal variability, from diel to interannual scales, in the
24 carbonate system (specifically pH and *p*CO₂) at the Aransas Ship Channel located in
25 northwestern Gulf of Mexico. Using other co-located environmental sensors, we also
26 explored the driving factors of that variability. Both sampling methods demonstrated
27 significant seasonal variability at the location, with highest pH (lowest *p*CO₂) in the
28 winter and lowest pH (highest *p*CO₂) in the summer. Significant diel variability was also
29 evident from sensor data, but the time of day with elevated *p*CO₂/depressed pH was not
30 consistent across the entire monitoring period, sometimes reversing from what would be
31 expected from a biological signal. Though seasonal and diel fluctuations were smaller
32 than many other areas previously studied, carbonate chemistry parameters were among
33 the most important environmental parameters to distinguish between time of day and
34 between seasons. It is evident that temperature, biological activity, freshwater inflow, and
35 tide level (despite the small tidal range) are all important controls on the system, with
36 different controls dominating at different time scales. The results suggest that the
37 controlling factors of the carbonate system may not be exerted equally on both pH and
38 *p*CO₂ on diel timescales, causing separation of their diel or tidal relationships during

39 certain seasons. Despite known temporal variability on shorter timescales, discrete
40 sampling was generally representative of the average carbonate system and average air-
41 sea CO₂ flux on a seasonal and annual basis when compared with sensor data.

42 **1. Introduction**

43 Coastal waters, especially estuaries, experience substantial spatial and temporal
44 heterogeneity in water chemistry—including carbonate chemistry parameters such as pH
45 and partial pressure of CO₂ (*p*CO₂)—due to the diversity of co-occurring biogeochemical
46 and anthropogenic processes (Hofmann et al., 2011; Waldbusser and Salisbury, 2014).

47 Carbonate chemistry is important because an addition of CO₂ acidifies seawater, and
48 acidification can negatively affect marine organisms (Barton et al., 2015; Bednaršek et
49 al., 2012; Ekstrom et al., 2015; Gazeau et al., 2007; Gobler and Talmage, 2014).

50 Additionally, despite the small surface area of coastal waters relative to the global ocean,
51 coastal waters are recognized as important contributors in global carbon cycling (Borges,
52 2005; Cai, 2011; Laruelle et al., 2018).

53 While carbonate chemistry, acidification, and air-sea CO₂ fluxes are relatively
54 well studied and understood in open ocean environments, large uncertainties remain in
55 coastal environments. Estuaries are especially challenging to fully understand because of
56 the heterogeneity between and within estuaries that is driven by diverse processes
57 operating on different time scales such as river discharge, nutrient and organic matter
58 loading, stratification, and coastal upwelling (Jiang et al., 2013; Mathis et al., 2012). The
59 traditional sampling method for carbonate system characterization involving discrete
60 water sample collection and laboratory analysis is known to lead to biases in average
61 *p*CO₂ and CO₂ flux calculations due to daytime sampling that neglects to capture diel

62 variability (Li et al., 2018). Mean diel ranges in pH can exceed 0.1 unit in many coastal
63 environments, and especially high diel ranges (even exceeding 1 pH unit) have been
64 reported in biologically productive areas or areas with higher mean $p\text{CO}_2$ (Challener et
65 al., 2016; Cyronak et al., 2018; Schulz and Riebesell, 2013; Semesi et al., 2009; Yates et
66 al., 2007). These diel ranges can far surpass the magnitude of the changes in open ocean
67 surface waters that have occurred since the start of the industrial revolution and rival
68 spatial variability in productive systems, indicating their importance for a full
69 understanding of the carbonate system.

70 Despite the need for high-frequency measurements, sensor deployments have
71 been limited in estuarine environments (especially compared to their extensive use in the
72 open ocean) because of the challenges associated with **varying conditions**, biofouling,
73 and sensor drift (Sastri et al., 2019). Carbonate chemistry monitoring in the Gulf of
74 Mexico (GOM), has been relatively minimal compared to the United States east and west
75 coasts. The GOM estuaries currently have less exposure to concerning levels of
76 acidification than other estuaries because of their high temperatures (causing water to
77 hold less CO_2 and support high productivity year-round) and often suitable river
78 chemistries (i.e., relatively high buffer capacity) (McCutcheon et al., 2019; Yao et al.,
79 2020). However, respiration-induced acidification is present in both the open GOM (e. g.,
80 subsurface water influenced by the Mississippi River Plume and outer shelf region near
81 the Flower Garden Banks National Marine Sanctuary) and GOM estuaries, and most
82 estuaries in the northwestern GOM have also experienced long-term acidification (Cai et
83 al., 2011; Hu et al., 2018, 2015; Kealoha et al., 2020; McCutcheon et al., 2019; Robbins
84 and Lisle, 2018). This **known acidification** as well as the relatively high CO_2 efflux from

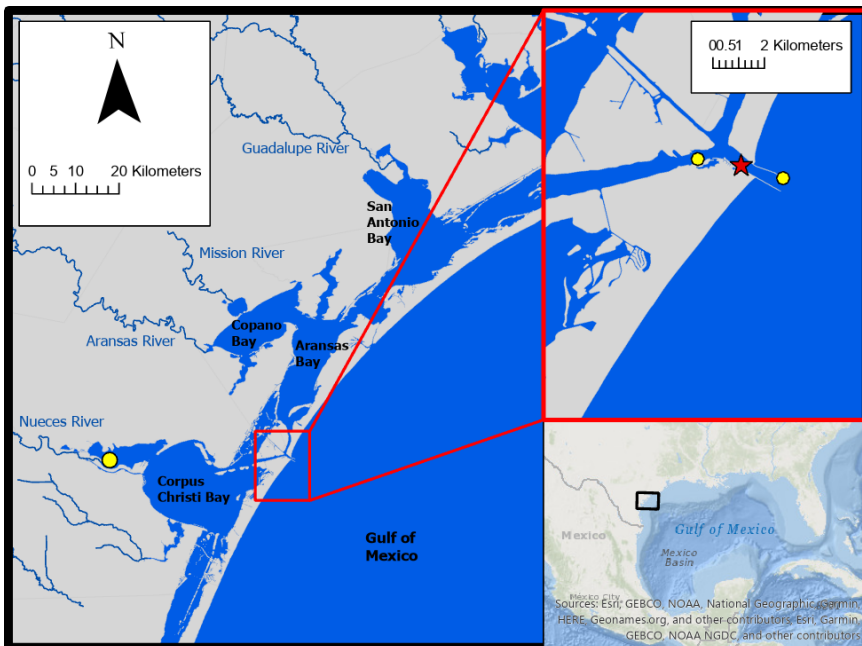
85 the estuaries of the northwest GOM illustrates the necessity to study the baseline
86 variability and driving factors of carbonate chemistry in the region. In this study, we
87 explored temporal variability in the carbonate system in Aransas Ship Channel (ASC)—a
88 tidal inlet where the lagoonal estuaries meet the coastal waters in a semi-arid region of
89 the northwestern GOM—using both discrete bottle sample collection and hourly sensor
90 measurements, and we explored the driving factors of that variability using data from
91 other co-located environmental sensors. The characterization of carbonate chemistry and
92 consideration of regional drivers can provide context to acidification and its impacts and
93 improved estimates of air-sea CO₂ fluxes.

94 **2. Materials and Methods**

95 *2.1 Location*

96 Autonomous sensor monitoring and discrete water sample collections for
97 laboratory analysis of carbonate system parameters were performed in the Aransas Ship
98 ChannelASC (ASC, located at 27°50'17"N, 97°3'1"W). ASC is one of the few permanent
99 tidal inlets that intersect a string of barrier islands and connect the GOM coastal waters
100 with the lagoonal estuaries in the northwest GOM (Fig. 1). ASC provides the direct
101 connection between the northwestern GOM and the Mission-Aransas Estuary (Copano
102 and Aransas Bays) to the north and Nueces Estuary (Nueces and Corpus Christi Bays) to
103 the south (Fig. 1). The region is microtidal, with a small tidal range relative to many other
104 estuaries, ranging from ~ 0.6 m tides on the open coast to less than 0.3 m in upper
105 estuaries (Montagna et al., 2011). Mission-Aransas Estuary (MAE) is fed by two small
106 rivers, the Mission (1787 km² drainage basin) and Aransas (640 km² drainage basin)
107 Rivers (<http://waterdata.usgs.gov/>), which both experience low base flows punctuated by

108 periodic high flows during storm events. MAE has an average residence time of one year
109 (Solis and Powell, 1999), so there is a substantial lag between time of rainfall and
110 riverine delivery to ASC in the lower estuary. A significant portion of riverine water
111 flowing into Aransas Bay originates from the larger rivers further northeast on the Texas
112 coast via the Intracoastal Waterway (i.e., Guadalupe River (26,625 km² drainage basin)
113 feeds San Antonio Bay and has a much shorter residence time of nearly 50 days) (Solis
114 and Powell, 1999; USGS, 2001).



115
116 **Figure 1.** Study area. The location of monitoring in the Aransas Ship Channel (red star)
117 and the locations of NOAA stations used for wind data (yellow circles) are shown.

118
119 *2.2 Continuous Monitoring*

120 Autonomous sensor monitoring (referred to throughout as continuous monitoring)
121 of pH and $p\text{CO}_2$ was conducted from Nov. 8, 2016 to Aug. 23, 2017 at the University of

122 Texas Marine Science Institute's research pier in ASC. Hourly pH data were collected
123 using an SAtlantic® SeaFET pH sensor (on total pH scale) and hourly $p\text{CO}_2$ data were
124 collected using a Sunburst® SAMI-CO₂. Hourly temperature and salinity data were
125 measured by a YSI® 600OMS V2 sonde. All hourly data were single measurements taken
126 on the hour. The average difference between sensor pH and discrete quality assurance
127 samples measured spectrophotometrically in the lab was used to establish a correction (-
128 0.05) based on a single calibration point across the entire sensor pH dataset (Bresnahan et
129 al., 2014). See supplemental materials for additional sensor deployment and quality
130 assurance information.

131 *2.3 Discrete Sample Collection and Sample Analysis*

132 Long-term monitoring via discrete water sample collection was conducted at ASC
133 from May 2, 2014 to February 25, 2020 (in addition to the discrete, quality assurance
134 sample collections). Sampling A single, discrete, surface water sample was conducted
135 collected every two weeks during the summer months and monthly during the winter
136 months from a small vessel at a station near (<20 m from) the sensor deployment. Water
137 sample collection followed standard protocol for ocean carbonate chemistry studies
138 (Dickson et al., 2007). Ground glass borosilicate bottles (250 mL) were filled with
139 surface water and preserved with 100 μL saturated mercury chloride (HgCl_2). Apiezon®
140 grease was applied to the bottle stopper, which was then secured to the bottle using a
141 rubber band and a nylon hose clamp.

142 These samples were used for laboratory dissolved inorganic carbon (DIC) and pH
143 measurements. DIC was measured by injecting 0.5 mL of sample into 1 ml 10% H_3PO_4
144 (balanced by 0.5 M NaCl) with a high-precision Kloehn syringe pump. The CO_2 gas

145 produced through sample acidification was then stripped using high-purity nitrogen gas
146 and carried into a Li-Cor infrared gas detector. DIC analyses had a precision of 0.1%.
147 Certified Reference Material (CRM) was used to ensure the accuracy of the analysis
148 (Dickson et al. 2003). For samples with salinity>20, pH was measured using a
149 spectrophotometric method at $25 \pm 0.1^\circ\text{C}$ (Carter et al. 2003) and the Douglas and Byrne
150 (2017) equation. Analytical precision of the spectrophotometric method for pH
151 measurement was ± 0.0004 pH units. A calibrated Orion Ross glass pH electrode was
152 used to measure pH at $25 \pm 0.1^\circ\text{C}$ for samples with salinity<20, and analytical precision
153 was ± 0.01 pH units. All pH values obtained using the potentiometric method were
154 converted to total scale at *in situ* temperature (Millero 2001). Salinity of the discrete
155 samples was measured using a benchtop salinometer calibrated by MilliQ water and a
156 known salinity CRM. For discrete samples, $p\text{CO}_2$ was calculated in CO2Sys for Excel
157 using laboratory-measured salinity, DIC, pH, and *in situ* temperature for calculations.
158 Carbonate speciation calculations were done using Millero (2010) carbonic acid
159 dissociation constants (K_1 and K_2), Dickson (1990) bisulfate dissociation constant, and
160 Uppström (1974) borate concentration.

161 *2.4 Calculation of CO₂ fluxes*

162 Equation 1 was used for air-water CO₂ flux calculations (Wanninkhof, 1992;
163 Wanninkhof et al., 2009). Positive flux values indicate CO₂ emission from the water into
164 the atmosphere (the estuary acting as a source of CO₂), and negative flux values indicate
165 CO₂ uptake by the water (the estuary acting as a sink for CO₂).

166
$$F = k K_0 (p\text{CO}_{2,w} - p\text{CO}_{2,a}) \quad (1)$$

167 where k is the gas transfer velocity (in m d^{-1}), K_0 (in $\text{mol l}^{-1} \text{ atm}^{-1}$) is the solubility
168 constant of CO_2 (Weiss, 1974), and $p\text{CO}_{2,\text{w}}$ and $p\text{CO}_{2,\text{a}}$ are the partial pressure of CO_2 (in
169 μatm) in the water and air, respectively.

170 We used the wind speed parameterization for gas transfer velocity (k) from Jiang
171 et al. (2008) converted from cm h^{-1} to m d^{-1} , which is thought to be the best estuarine
172 parameterization at this time (Crosswell et al., 2017), as it is a composite of k over
173 several estuaries. The calculation of k requires a windspeed at 10 m above the surface, so
174 windspeeds measured at 3 m above the surface were converted using the power law wind
175 profile (Hsu, 1994; Yao and Hu, 2017). To assess uncertainty, other parameterizations
176 with direct applications to estuaries in the literature were also used to calculate CO_2 flux
177 (Raymond and Cole 2001; Ho et al. 2006). We note that parameterization of k based on
178 solely windspeed is flawed because several additional parameters can contribute to
179 turbulence including turbidity, bottom-driven turbulence, water-side thermal convection,
180 tidal currents, and fetch (Wanninkhof 1992, Abril et al., 2009, Ho et al., 2104, Andersson
181 et al., 2017), however it is currently the best option for this system given the limited
182 investigations of CO_2 flux and contributing factors in estuaries.

183 Hourly averaged windspeed data for use in CO_2 flux calculations were retrieved
184 from the NOAA-controlled Texas Coastal Ocean Observation Network (TCOON;
185 <https://tidesandcurrents.noaa.gov/tcoon.html>). Windspeed data from the nearest TCOON
186 station (Port Aransas Station – located directly in ASC, < 2 km inshore from our
187 monitoring location) was prioritized when data were available. During periods of missing
188 windspeed data at the Port Aransas Station, wind speed data from TCOON's Aransas
189 Pass Station (< 2 km offshore from monitoring location) were next used, and for all

190 subsequent gaps, data from TCOON's Nueces Bay Station (~ 40 km away) were used
191 (Fig. 1; additional discussion of flux calculation and windspeed data can be found in
192 supplementary materials). For flux calculations from continuous monitoring data, each
193 hourly measurement of $p\text{CO}_2$ was paired with the corresponding hourly averaged
194 windspeed. For flux calculations from discrete sample data, the $p\text{CO}_2$ calculated for each
195 sampled day was paired with the corresponding daily averaged windspeed (calculated
196 from the retrieved hourly averaged windspeeds).

197 Monthly mean atmospheric xCO_2 data (later converted to $p\text{CO}_2$) for flux
198 calculations were obtained from NOAA's flask sampling network of the Global
199 Monitoring Division of the Earth System Research Laboratory at the Key Biscayne (FL,
200 USA) station. Global averages of atmospheric xCO_2 were used when Key Biscayne data
201 were unavailable. Each $p\text{CO}_2$ observation (whether using continuous or discrete data)
202 was paired with the corresponding monthly averaged xCO_2 for flux calculations.
203 Additional information and justification are available in supplemental materials.

204 *2.5 Additional data retrieval and data processing to investigate carbonate system*

205 *variability and controls*

206 All reported annual mean values are seasonally weighted to account for
207 disproportional sampling between seasons. However, reported annual standard deviation
208 is associated with the un-weighted, arithmetic mean (Table S1). Temporal variability was
209 investigated in the form of seasonal and diel variability (Tables S1, S2, S3). For seasonal
210 analysis, December to February was considered winter, March to May was considered
211 spring, June to August was considered summer, and September to November was
212 considered fall. It is important to note that the Fall season had much fewer continuous

213 sensor observations than other seasons because of the timing of sensor deployment. For
214 diel comparisons, daytime and nighttime ~~variables~~ were defined as 09:00-15:00 local
215 standard time and 21:00-03:00 local standard time, respectively, based on the 6-hour
216 periods with highest and lowest photosynthetically active radiation (PAR; data from co-
217 located sensor, obtained from the Mission-Aransas National Estuarine Research Reserve
218 (MANERR) at <https://missionaransas.org/science/download-data>). Diel ranges in
219 parameters were calculated (daily maximum minus daily minimum) and only reported for
220 days with the full 24 hours of hourly measurements (176 out of 262 measured days) to
221 ensure that data gaps did not influence the diel ranges (Table S3).

Controls on $p\text{CO}_2$ from thermal and non-thermal (i.e., combination of physical and biological) processes were investigated following Takahashi et al. (2002) over annual, seasonal, and daily time scales using both continuous and discrete data. Over any given time period, this method uses the ratio of the ranges of temperature-normalized $p\text{CO}_2$ ($p\text{CO}_{2,\text{nt}}$, Eq. 2) and the mean annual $p\text{CO}_2$ perturbed by the difference between mean and observed temperature ($p\text{CO}_{2,\text{t}}$, Eq. 3) to calculate the relative influence of non-thermal and thermal effects on $p\text{CO}_2$ (T/B, Eq. 4). When calculating annual T/B values with discrete data, only complete years (sampling from January to December) were included (2014 and 2020 were omitted). When calculating daily T/B values with continuous data, only complete days (24 hourly measurements) were included.

$$p_{\text{CO}_2 \text{ int}} = p_{\text{CO}_2 \text{ obs}} \times \exp[\delta \times (T_{\text{mean}} - T_{\text{obs}})] \quad (2)$$

$$p_{\text{CO}_2, \text{f}} = p_{\text{CO}_2, \text{mean}} \times \exp[\delta \times (T_{\text{obs}} - T_{\text{mean}})] \quad (3)$$

234 where the value for δ ($0.0411 \text{ } ^\circ\text{C}^{-1}$), which represents average $[\partial \ln p\text{CO}_2 / \partial$
 235 Temperature] from field observations, was taken directly from Yao and Hu (2017), T_{obs} is

236 the observed temperature, and T_{mean} is the mean temperature over the investigated time
237 period.

$$238 T/B = \frac{\max(pCO_{2,thermal}) - \min(pCO_{2,thermal})}{\max(pCO_{2,non-thermal}) - \min(pCO_{2,non-thermal})} \quad (4)$$

239 Where a T/B greater than one indicates that temperature's control on pCO_2 is greater than
240 the control from non-thermal factors and a T/B less than one indicates that non-thermal
241 factors' control on pCO_2 is greater than the control from temperature.

242 Tidal control on parameters was investigated using our continuous monitoring
243 data and tide level data obtained from NOAA's Aransas Pass Station (the Aransas Pass
244 Station used for windspeed data, < 2 km offshore from monitoring location, Fig. 1) at
245 [https://tidesandcurrents.noaa.gov/waterlevels.html?id=8775241&name=Aransas,%20Ara
246 nsas%20Pass&state=TX](https://tidesandcurrents.noaa.gov/waterlevels.html?id=8775241&name=Aransas,%20Aransas%20Pass&state=TX). Hourly measurements of water level were merged with our
247 sensor data by date and hour. Given that there were gaps in available water level
248 measurements (and no measurements prior to December 20, 2016), the usable dataset was
249 reduced from 6088 observations to 5121 observations and fall was omitted from analyses.
250 To examine differences between parameters during high tide and low tide, we defined
251 high tide as tide level greater than the third quartile tide level value and low tide as a tide
252 level less than the first quartile tide level value.

253 Other factors that may exert control on the carbonate system were investigated
254 through parameter relationships. In addition to previously discussed tide and windspeed
255 data, we obtained dissolved oxygen (DO), PAR, turbidity, and chlorophyll fluorescence
256 data from MANERR-deployed environmental sensors that were co-located at our
257 monitoring location (obtained from <https://missionaransas.org/science/download-data>).
258 Given that MANERR data are all measured in the bottom water (>5 m) while our sensors

259 were measuring surface waters, we excluded the observations with significant water
260 column stratification (defined as a salinity difference > 3 between surface water and
261 bottom water) from analyses. Omitting stratified water reduced our continuous dataset
262 from 6088 to 5524 observations (removing 260 winter, 133 spring, 51 summer, and 120
263 fall observations), and omitting observations where there were no MANERR data to
264 determine stratification further reduced the dataset to 4112 observations. Similarly,
265 removing instances of stratification reduced discrete sample data from 104 to 89 surface
266 water observations.

267 *2.6 Statistical Analyses*

268 All statistical analyses were performed in R, version 4.0.3 (R Core Team, 2020).
269 To investigate differences between daytime and nighttime parameter values (temperature,
270 salinity, pH, $p\text{CO}_2$, and CO_2 flux) using continuous monitoring data across the full
271 sampling period and within each season, paired t -tests were used, pairing each respective
272 day's daytime and nighttime values (Table S3). We also used loess models (locally
273 weighted polynomial regression) to identify changes in diel patterns over the course of
274 our monitoring period.

275 Two-way ANOVAs were used to examine differences in parameter means
276 between seasons and between monitoring methods (Table S2). Since there were
277 significant interactions (between season and sampling type factors) in the two-way
278 ANOVAs for each individual parameter (Table S2), differences between seasons were
279 investigated within each monitoring method (one-way ANOVAs) and the differences
280 between monitoring methods were investigated within each season (one-way ANOVAs).
281 For the comparison of monitoring methods, we included both the full discrete sampling

282 data as well as a subset of the discrete sampling data to overlap with the continuous
283 monitoring period (referred to throughout as reduced discrete data or Dc) along with the
284 continuous data. To interpret differences between monitoring methods, a difference in
285 means between the continuous monitoring and discrete monitoring datasets would only
286 indicate that the 10-month period of continuous monitoring was not representative of the
287 5+ year period that discrete samples have been collected, but a difference in means
288 between the continuous data and discrete sample data collected during the continuous
289 monitoring period represents discrepancies between types of monitoring. Post-hoc
290 multiple comparisons (between seasons within sampling types and between sampling
291 types within seasons) were conducted using the Westfall adjustment (Westfall, 1997).

292 Differences in parameters between high tide and low tide conditions were
293 investigated using a two-way ANOVA to model parameters based on tide level and
294 season. In models for each parameter, there was a significant interaction between tide
295 level and season factors (based on $\alpha=0.05$, results not shown), thus t-tests were used
296 (within each season) to examine differences in parameters between high and low tide
297 conditions. Note that fall was omitted from this analysis because tide data were only
298 available at the location beginning December 20, 2016. Sample sizes were the same for
299 each parameter (High tide – winter: 354, spring: 569, summer: 350; Low tide – winter:
300 543, spring: 318, summer: 415).

301 Additionally, to gain insight to carbonate system controls through correlations, we
302 conducted Pearson correlation analyses to examine individual correlations of pH and
303 $p\text{CO}_2$ (both continuous and discrete) with other environmental parameters (Table S5).

304 To better understand overall system variability over different time scales, we used
305 a linear discriminant analysis (LDA), a multivariate statistic that allows dimensional
306 reduction, to determine the linear combination of environmental parameters (individual
307 parameters reduced into linear discriminants, LDs) that allow the best differentiation
308 between day and night as well as between seasons. We included $p\text{CO}_2$, pH, temperature,
309 salinity, tide level, wind speed, total PAR, DO, turbidity, and fluorescent chlorophyll in
310 this analysis. All variables were centered and scaled to allow direct comparison of their
311 contribution to the system variability. The magnitude (absolute value) of coefficients of
312 the LDs (Table 1) represents the relative importance of each individual environmental
313 parameter in the best discrimination between day and night and between seasons, i.e., the
314 greater the absolute value of the coefficient, the more information the associated
315 parameter can provide about whether the sample came from day or night (or winter,
316 spring, or summer). Only one LD could be created for the diel variability (since there are
317 only two classes to discriminate between – day and night). Two LDs could be created for
318 the seasonal variability (since there were three classes to discriminate between – fall was
319 omitted because of the lack of tidal data), but we chose to only report the coefficients for
320 LD1 given that LD1 captured 95.64% of the seasonal variability.

321

322 **3. Results**

323 *3.1 Seasonal variability*

324 Both the continuous and discrete data showed substantial seasonal variability for
325 all parameters (Fig. 2, Tables S1 and S2). All discrete sample results reported here are for
326 the entire 5+ years of monitoring; the subset of discrete sample data that overlaps with

327 the continuous monitoring period will be addressed only in the discussion for method
328 comparisons (Section 4.1.1). Both continuous and discrete data demonstrate significant
329 differences in temperature between each season, with the highest temperature in summer
330 and the lowest in winter (Tables S1 and S2). Mean salinity during sampling periods was
331 highest in the summer and lowest in the fall (Table S1). Significant differences in
332 ~~seasonal~~ salinity occurred between all seasons except spring and winter for continuous
333 data, but only summer differed from other seasons based on discrete data (Tables S1 and
334 S2).

335 Carbonate system parameters also varied seasonally (Fig. 2). For both continuous
336 and discrete data, winter had the highest seasonal pH (8.19 ± 0.08 and 8.162 ± 0.065 ,
337 respectively) and lowest seasonal $p\text{CO}_2$ (365 ± 44 μatm and 331 ± 39 μatm ,
338 respectively), while summer had the lowest seasonal pH (8.05 ± 0.06 and 7.975 ± 0.046 ,
339 respectively) and highest seasonal $p\text{CO}_2$ (463 ± 48 μatm and 511 ± 108 , respectively)
340 (Fig. 2, Table S1). All seasonal differences in pH and $p\text{CO}_2$ were significant, except for
341 the discrete data spring versus fall for both parameters (Table S2).

342
343

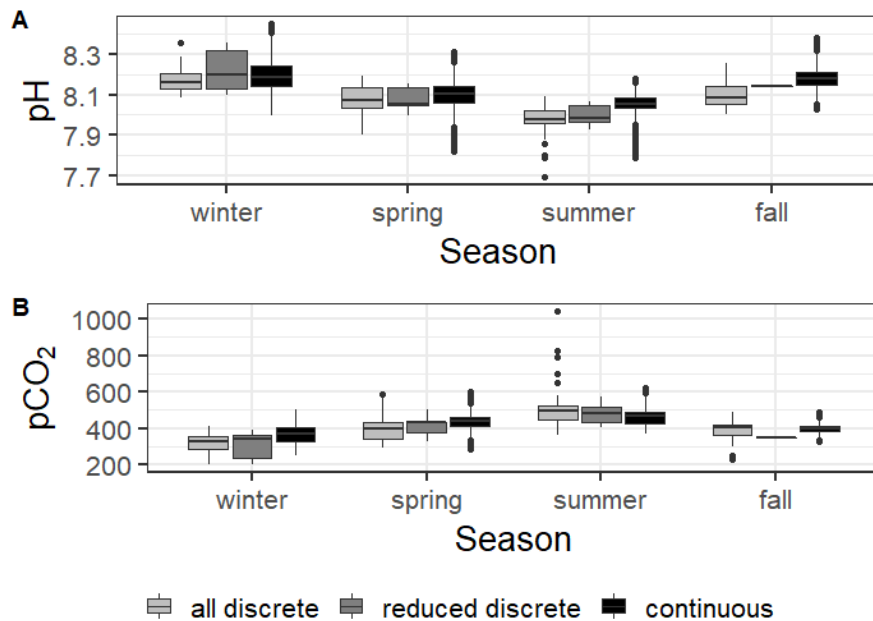
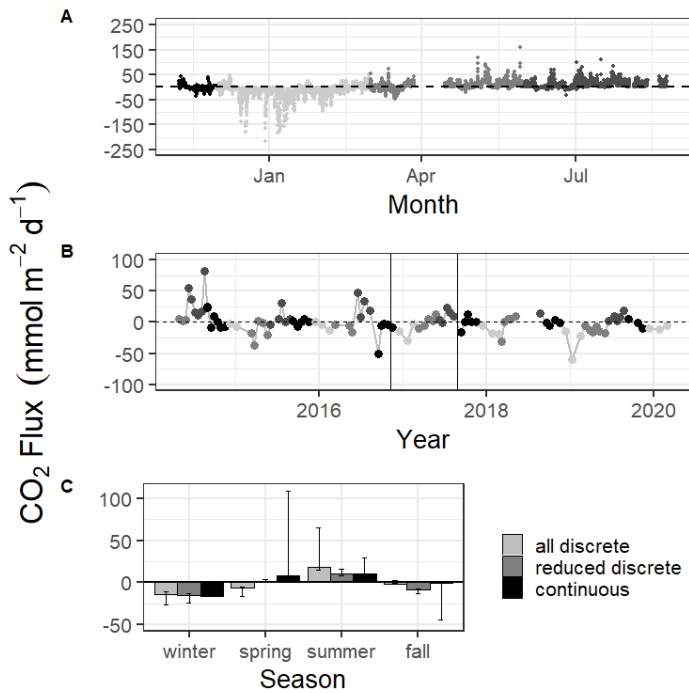


Figure 2. Boxplots of seasonal variability in pH and $p\text{CO}_2$ using all discrete data, reduced discrete data (to overlap with continuous monitoring, Nov. 8 2016 – Aug 23, 2017), and continuous sensor data.

344
345
346
347
348

349 Mean CO_2 flux differed by season (Fig. 3, Tables S1 and S2). Both continuous
350 and discrete data records resulted in net negative CO_2 fluxes during fall and winter
351 months, with winter being most negative. Both methods reported a net positive flux for
352 summer, while spring fluxes were positive according to continuous data and negative
353 according to the 5+ years of discrete data (Fig. 3, Table S1). Annual net CO_2 fluxes were
354 near zero (Table S1).

355



356
 357 **Figure 3.** CO₂ flux calculated over the sampling periods from continuous (A) and
 358 discrete (B) data. Gray scale in (A) and (B) denote different seasons. Vertical lines in (B)
 359 denote the time period of continuous monitoring. (C) shows the seasonal mean CO₂ flux.
 360 Error bars represent mean CO₂ flux using Ho (2006) and Raymond and Cole (2001)
 361 windspeed parameterizations.
 362

363 Results of the LDA incorporated carbonate system parameters along with
 364 additional environmental parameters to get a full picture of system variability over
 365 seasonal timescales (Table 1). The most important parameter in system variability that
 366 allowed differentiation between seasons was temperature (Table 1, Seasonal LD1), as
 367 would be expected with the clear seasonal temperature fluctuations (Fig. S1E). The
 368 second most important parameter for seasonal differentiation was chlorophyll, likely
 369 indicating clear seasonal phytoplankton blooms. The carbonate chemistry also played a

370 critical role in seasonal differentiation, as $p\text{CO}_2$ was the third most important factor
371 (Table 1).

372 **Table 1.** Coefficients of linear discriminants (LD) from LDA using continuous sensor
373 data and other environmental parameters. Discriminants for both diel and seasonal
374 variability shown.

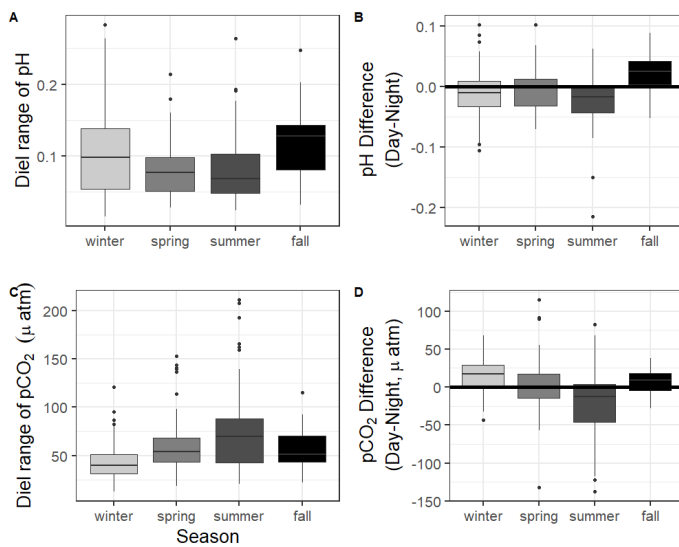
	Seasonal	Diel
	LD1	LD1
Temperature (°C)	-3.53	0.54
Salinity	0.04	0.15
$p\text{CO}_2$ (μatm)	-0.29	-0.16
pH	0.10	0.06
Tide Level (m)	-0.24	0.10
Wind speed (ms ⁻¹)	0.05	-0.00
Total PAR	-0.07	-2.29
DO (mg L ⁻¹)	0.09	-0.08
Turbidity	0.15	-0.06
Fluor. Chlorophyll	-0.40	0.14

375
376 *3.2 Diel variability*

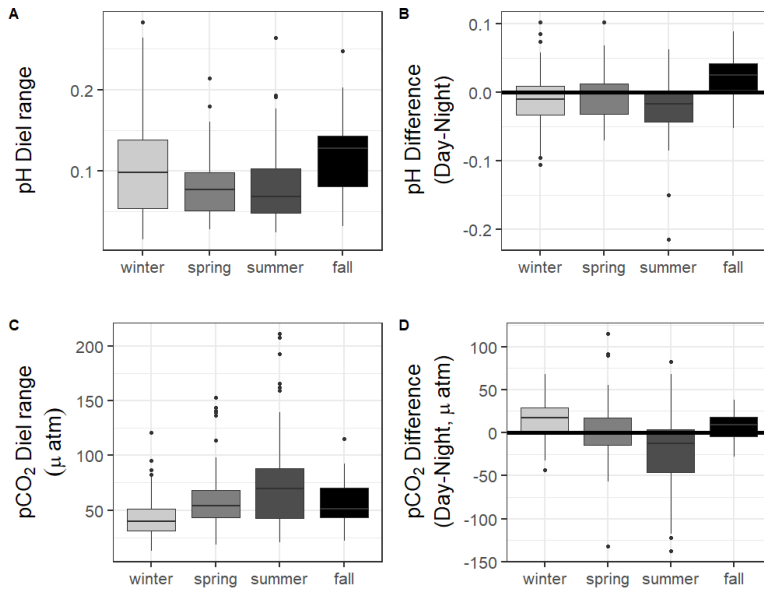
377 The 10 months of in-situ continuous monitoring revealed that there was
378 substantial diel variability in measured parameters (Fig. 4, Table S3). Temperature had a
379 mean diel range of $1.3 \pm 0.8^\circ\text{C}$ (Table S3). Daytime and nighttime temperature differed
380 significantly during the summer and fall months, with higher temperatures at night for
381 both seasons (Table S3). The mean diel range of salinity was 3.4 ± 2.7 (Table S3).
382 Daytime and nighttime salinity differed significantly during the winter and fall months,
383 with higher salinities at night for both seasons. The mean diel range of pH was $0.09 \pm$
384 0.05 (Table S3). Daytime and nighttime pH differed significantly during the winter,
385 summer, and fall, with nighttime pH significantly higher during summer and winter and
386 lower during fall (Fig. 4, Table S3). The mean diel range of $p\text{CO}_2$ was 58 ± 33 μatm (Fig.
387 4, Table S3). Daytime and nighttime $p\text{CO}_2$ differed significantly during the winter and
388 summer months, with nighttime $p\text{CO}_2$ significantly higher during the summer and lower
389 during the winter (Fig. 4, Table S3). No significant difference in daytime and nighttime

390 DO were observed during any season (Fig. 5F; paired t-tests, winter $p = 0.1573$, spring p
391 $= 0.4877$, summer $p = 0.794$).

392 Loess models that investigated the evolution of day-night difference in parameters
393 revealed that other environmental parameters, including salinity, temperature, and tide
394 level, also had diel patterns that varied over the duration of our continuous monitoring
395 (Fig. 5).



896

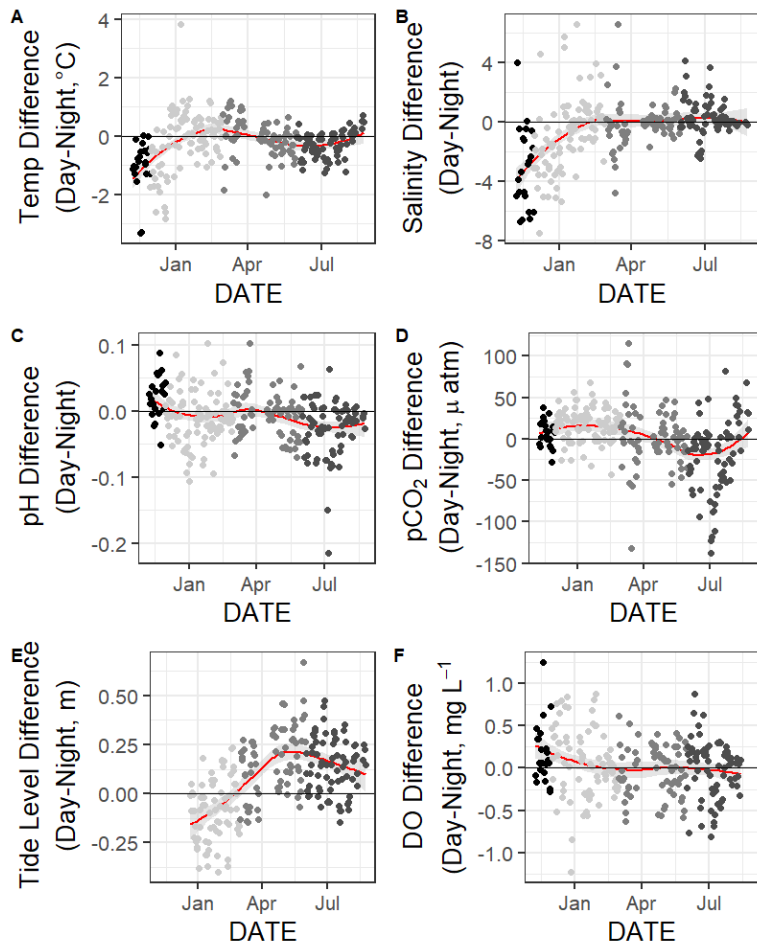


397

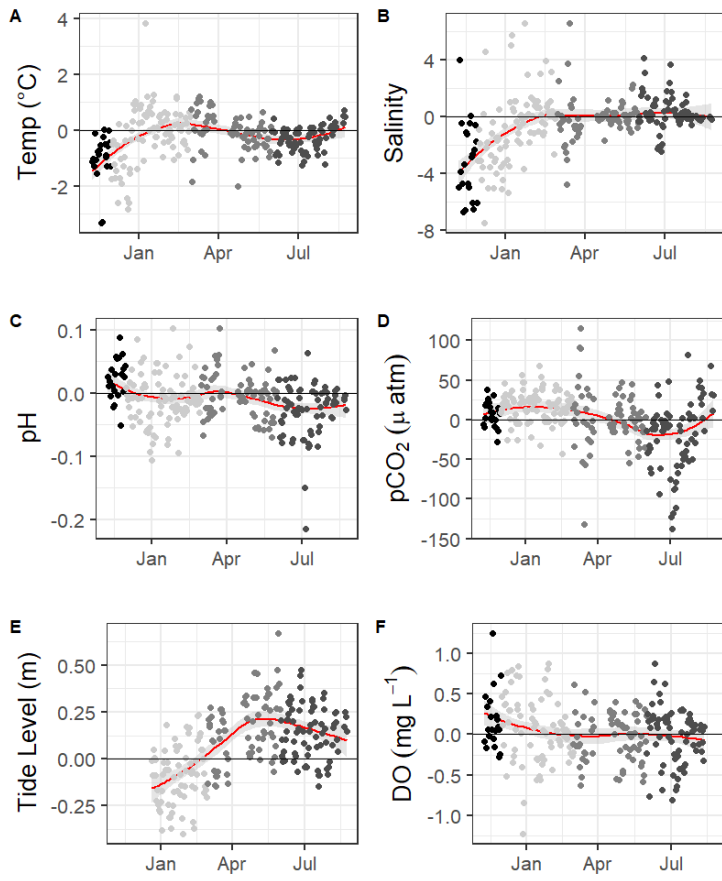
398 **Figure 4.** Boxplots of the diel range (maximum minus minimum) and difference in daily
 399 parameter mean daytime minus nighttime measurements for pH and $p\text{CO}_2$ from
 400 continuous sensor data.

401

402 CO_2 flux also fluctuated on a daily scale, with a mean diel range of 34.1 ± 29.0
 403 $\text{mmol m}^{-2} \text{d}^{-1}$ (Table S3). However, there was not a significant difference in CO_2 flux of
 404 daytime versus nighttime hours for the entire monitoring period or any individual season
 405 based on $\alpha=0.05$ (paired t-test, Table S3).



406
407



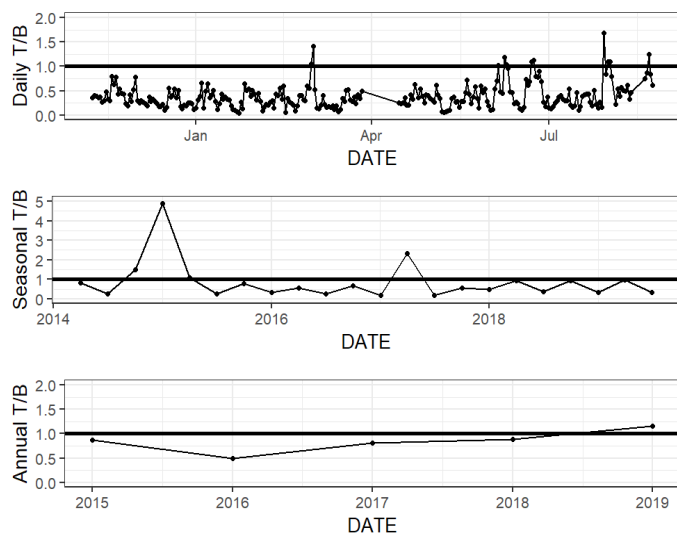
408
 409 **Figure 5.** Loess models (red line) and their confidence intervals (gray bands) showing the
 410 difference in daily parameter mean daytime mean minus nighttime mean measurements.
 411 The gray scale of the data points represents the four seasons over which data were
 412 collected. Data span from Nov 8, 2016 to Aug 3, 2017, except for the tide data, which
 413 began December 20, 2016.

414
 415 Results of the LDA for differentiation between daytime and nighttime conditions
 416 revealed that the most important factor was PAR, as would be expected (Table 1, Diel
 417 LD1). Temperature was the second most important factor to differentiate between day
 418 and night. The carbonate chemistry also played a critical role in day/night differentiation,

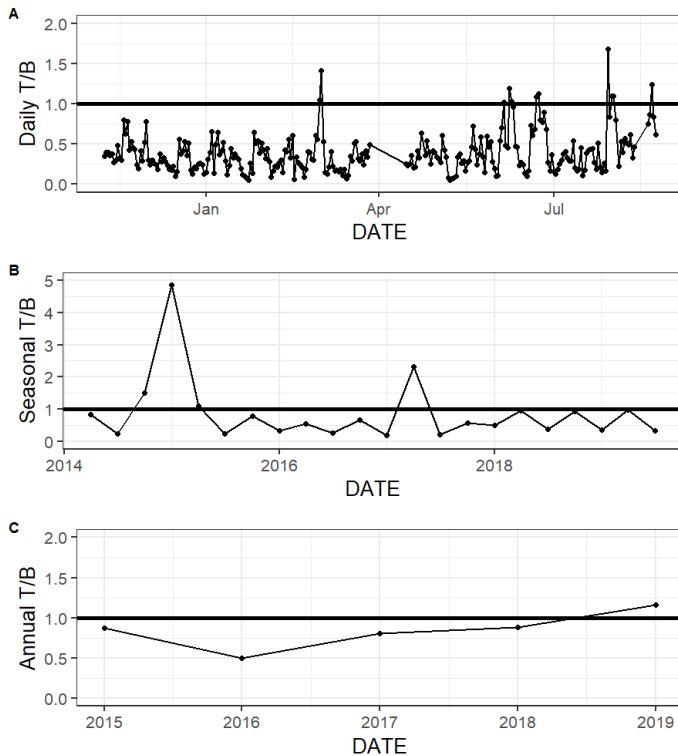
419 as $p\text{CO}_2$ was the third most important parameter, providing more evidence for
420 differentiation between day and night than other parameters that would be expected to
421 vary on a diel timescale (e.g., chlorophyll and DO) (Table 1).

422 *3.3 Controlling factors and correlates*

423 The relative influence of thermal and non-thermal factors (T/B) in controlling
424 $p\text{CO}_2$ varied over different time scales (Fig. 6, Table S4). Based on continuous data, non-
425 thermal processes generally exerted more control than thermal processes (T/B<1) over
426 the entire 5+ years of discrete monitoring, within each season, and over most (167/178)
427 days (Fig. 6, Table S4). Annual T/B from discrete data ranged from 0.50 to 1.16, with
428 only one of the five sampled years having T/B greater than one (i.e., more thermal
429 influence; Table S4). While most individual seasons that were sampled experienced
430 stronger non-thermal control on $p\text{CO}_2$ (T/B <1), the only season that never experienced
431 stronger thermal control was summer, with summer T/B values ranging from 0.21 – 0.35
432 for the 6 sampled years (Table S4).



433



434
 435 **Figure 6.** Thermal versus non-thermal control on $p\text{CO}_2$ daily (top A), seasonal (middle B),
 436 and annual (bottom C) time scales using both continuous sensor data (daily, from Nov 8,
 437 2016 to Aug 3, 2017) (daily) and discrete sample data (seasonal and annual, from May 2,
 438 2014–Feb 25, 2020 (seasonal and annual)).
 439

440 Tidal fluctuations seemed to have a significant effect on carbonate system
 441 parameters (Table 2). Both temperature and salinity were higher at low tide during the
 442 winter and summer months and higher at high tide during the spring. $p\text{CO}_2$ was higher
 443 during low tide during all seasons. pH was higher during high tide during the winter and
 444 summer, but this reversed during the spring, when pH was higher at low tide. CO_2 flux
 445 also varied with tidal fluctuations. CO_2 flux was higher (more positive or less negative) in

446 the low tide condition for all seasons (though the difference was not significant in
447 spring), i.e., the location was less of a CO₂ sink during low tide conditions in the winter
448 and more of a CO₂ source during low tide conditions in the summer.

449

450 **Table 2.** Mean and standard deviation of temperature, salinity, pH, pCO₂, and calculated
451 CO₂ flux (from continuous sensor measurements) during high and low tide conditions.

452

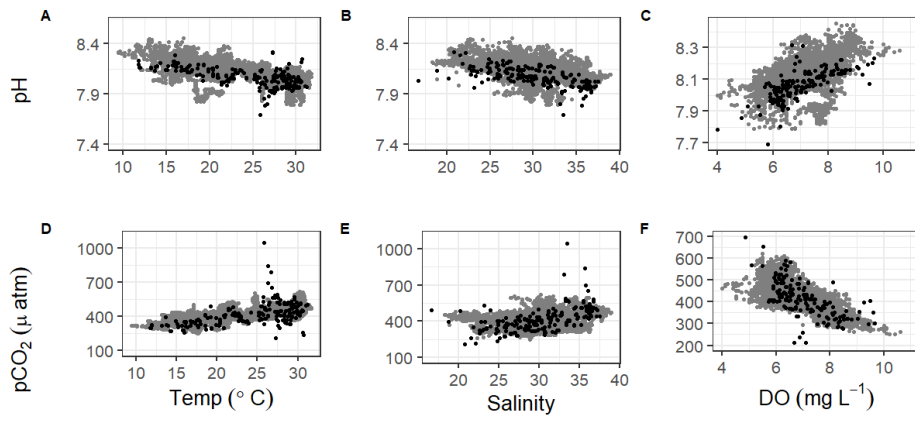
Parameter	Season	High Tide Mean	Low Tide Mean	Difference between tide levels, t-test p-value
Temperature (°C)	Winter	16.7 ± 1.7	17.6 ± 2.0	<0.0001
	Spring	24.4 ± 2.7	23.6 ± 2.7	<0.0001
	Summer	29.3 ± 0.5	30.1 ± 0.7	<0.0001
Salinity	Winter	30.2 ± 2.5	31.3 ± 2.9	<0.0001
	Spring	30.4 ± 1.9	30.0 ± 2.7	0.0071
	Summer	30.5 ± 2.4	34.5 ± 3.0	<0.0001
pH	Winter	8.20 ± 0.08	8.15 ± 0.06	<0.0001
	Spring	8.07 ± 0.09	8.10 ± 0.07	<0.0001
	Summer	8.08 ± 0.04	8.04 ± 0.06	<0.0001
pCO₂(μatm)	Winter	331 ± 40	378 ± 42	<0.0001
	Spring	435 ± 33	443 ± 50	0.0154
	Summer	419 ± 30	482 ± 48	<0.0001
CO₂ Flux (mmol m⁻² d⁻¹)	Winter	-33.0 ± 38.1	-11.7 ± 21.8	<0.0001
	Spring	7.4 ± 14.0	8.7 ± 14.8	0.2248
	Summer	1.8 ± 6.3	16.0 ± 14.5	<0.0001

453

454 Mean water level varied between all seasons; mean spring (highest) water levels
455 were on average 0.08 m higher than winter (lowest) water levels (ANOVA p<0.0001, fall
456 was not considered because of a lack of water level data). The mean daily tidal range
457 during our continuous monitoring period was 0.39 m ± 0.13 m, which did not
458 significantly differ between seasons (ANOVA p=0.739). However, the day-night
459 difference in tide level exhibited a strong seasonality, with spring and summer having
460 higher tide level during the daytime and winter having higher tide level during the
461 nighttime (Fig. 5).

462 There were significant correlations between carbonate system parameters (pH and
 463 $p\text{CO}_2$) and many of the other environmental parameters, including windspeed, DO,
 464 turbidity, and fluorescent chlorophyll (Figure 7, Table S5). Both the continuous and
 465 discrete sampling types indicate that pH has a significant negative relationship with both
 466 temperature and salinity and $p\text{CO}_2$ has a significant positive relationship with both
 467 temperature and salinity (Fig. 7). However, correlations with temperature were stronger
 468 for continuous data and correlations with salinity were stronger for discrete data (Table
 469 S5). The strongest correlations between continuous carbonate system data and all
 470 investigated environmental parameters were with DO (positive correlation with pH and
 471 negative correlation with $p\text{CO}_2$; Table S5). It is worth noting that there were no
 472 observations of hypoxia at our study site during our monitoring, with minimum DO
 473 levels of 3.9 mg L^{-1} and 4.0 mg L^{-1} for our continuous monitoring period and our discrete
 474 sampling period, respectively.

475
 476



477
 478 **Figure 7.** Correlations of pH and $p\text{CO}_2$ with temperature, salinity, and DO from
 479 continuous sensor data (gray) and all discrete data (black).

480

481 **Discussion**

482 *4.1 Comparing continuous monitoring and discrete sampling: Representative sampling in*
483 *a temporally variable environment*

484 Discrete water sample collection and analysis is the most common method that
485 has been employed to attempt to understand the carbonate system of estuaries. However,
486 it is difficult to know if these samples are representative of the spatial and temporal
487 variability in carbonate system parameters. While this time-series study cannot conclude
488 whether our broader sampling efforts in the MAE are representative of the spatial
489 variability in the estuary, it can investigate how representative our bimonthly to monthly
490 sampling is of the more high-frequency temporal variability that ASC experiences.

491 There were several instances where seasonal parameter means significantly
492 differed between the 10-month continuous monitoring period and the 5+ year discrete
493 sampling period (Table S2, $C \neq D$ or $D_c \neq D$) including temperature in the summer and
494 fall, salinity in the spring, pH in the summer and fall, and pCO_2 in winter, spring, and
495 summer. While clear seasonal variability was demonstrated for most parameters (using
496 both continuous and discrete data for the entire period), these differences between the 10-
497 month continuous monitoring period and our 5+ year monitoring period illustrate that
498 there is also interannual variability in the system. Therefore, short periods of monitoring
499 are unable to fully capture current baseline conditions.

500 During the continuous monitoring period (2016-2017), we found no significant
501 difference between sampling methods in the seasonal mean temperature, salinity, or
502 pCO_2 . The two sampling methods also resulted in the same mean pH for all seasons

503 except for summer, when the sensor data recorded a higher mean pH than discrete
504 samples (Tables S1 and S2). During this case, we can conclude that discrete monitoring
505 did not accurately represent the system variability that was able to be captured by the
506 sensor monitoring. However, given that most seasons did not show differences in pH or
507 $p\text{CO}_2$ between sampling methods, the descriptive statistics associated with the discrete
508 monitoring did a fair job of representing system means. This is evidence that long-term
509 discrete monitoring efforts, which are much more widespread in estuarine systems than
510 sensor deployments, can be generally representative of the system despite known
511 temporal variability on shorter time scales. However, further study would be needed to
512 determine if this applies throughout the system, as the upper estuary generally
513 experiences greater variability.

514 Understanding the relationships of pH and $p\text{CO}_2$ with temperature and salinity is
515 important in a system (Fig. 7). Based on the results of an Analysis of Covariance
516 (ANCOVA), the relationship (slope) of pH with both temperature and salinity and of
517 $p\text{CO}_2$ with salinity were not significantly different between types of monitoring
518 (considering the sensor deployment period only), supporting the effectiveness of long-
519 term discrete monitoring programs when sensors are unable to be deployed. However,
520 ANCOVA did reveal the relationship of $p\text{CO}_2$ with temperature is significantly different
521 (method:temp $p=0.0062$) between monitoring methods.

522 The high temporal resolution of sensor data is presumably better for estimating
523 CO_2 flux at a given location than discrete sampling. Previous studies have pointed out
524 that discrete sampling methods, which generally involve only daytime sampling, do not
525 adequately capture the diel variability in the carbonate system and may therefore lead to

526 underestimation-biased of CO₂ fluxes (Crosswell et al., 2017; Liu et al., 2016). However,
527 we found no significant difference (within any season) between CO₂ flux values
528 calculated with hourly sensor data versus single, discrete samples collected monthly to
529 twice monthly (Table S2, Fig. 3). Calculated CO₂ fluxes also did not significantly differ
530 between day and night during any season, despite some differences in *p*CO₂ (Table S3),
531 likely due to the large error associated with the calculation of CO₂ flux (Table S1, Fig. 3)
532 which will be further discussed below. Therefore, the expected underestimation of CO₂
533 flux based on diel variability of *p*CO₂ was not encountered at our study site, validating
534 the use of discrete samples for quantification of CO₂ fluxes (until methods with less
535 associated error are available). Even given less error in calculated flux, estimated fluxes
536 would likely not differ between methods on an annual scale (as *p*CO₂ did not), but CO₂
537 fluxes may differ on a seasonal scale since the differences between daytime and
538 nighttime *p*CO₂ were not consistent across seasons (Table S3, Fig. 4).

539 There are many factors contributing to error associated with CO₂ flux. There is
540 still large error associated with estimates of estuarine CO₂ flux because turbulent mixing
541 is difficult to model and turbulence is the main control on CO₂ gas transfer velocity, *k*, in
542 shallow water environments. Thus, our wind speed parameterization of *k* is imperfect and
543 likely the greatest source of error (Borges and Abril, 2011; Van Dam et al., 2019). Other
544 notable sources of error include the data treatment. For example, we chose to seasonally
545 weight the individual calculated flux values in the calculation of annual flux to account
546 for differences in sampling frequency between seasons. From continuous data, the
547 weighted average flux was 0.2 mmol m⁻² d⁻¹, although choosing not to seasonally weight
548 and simply look at the arithmetic mean of fluxes calculated directly from sampling dates

549 would have resulted in an annual CO₂ flux of -0.7 mmol m⁻² d⁻¹ for the same period.
550 Similarly, the weighted average flux from all 5+ years of discrete data was -0.9 mmol m⁻²
551 d⁻¹, but the arithmetic mean of fluxes would have resulted in an annual CO₂ flux of 0.2
552 mmol m⁻² d⁻¹ for the same period. Another source of error that could be associated with
553 the calculation of flux from the discrete data is the way in which wind speed data are
554 aggregated to be used in the windspeed parameterization. We decided to use daily
555 averages of the windspeed for calculations. Using the windspeed measured for the closest
556 time to our sampling time or the monthly averaged wind speed may have resulted in very
557 different flux values.

558

559 *4.2 Factors controlling temporal variability in carbonate system parameters*

560 Our study site had a relatively small range of pH and pCO₂ on both diel and
561 seasonal scales compared to other coastal regions (Challener et al., 2016; Yates et al.,
562 2007). This small variability is likely tied to a combination of the subtropical setting
563 (small temperature variability), the lower estuary position of our monitoring (further
564 removed from the already small freshwater influence), little ocean upwelling influence,
565 and the system's relatively high buffer capacity that results from the high alkalinity of the
566 freshwater endmembers (Yao et al., 2020). Just as the extent of hypoxia-induced
567 acidification was relatively low in Corpus Christi Bay because of the bay's high buffer
568 capacity (McCutcheon et al., 2019), the extent of pH fluctuation resulting from all
569 controlling factors at ASC would also be modulated by the region's high intrinsic buffer
570 capacity.

571 *4.2.1 Thermal and biological controls on carbonate chemistry*

- Formatted: Font: Italic
- Formatted: Indent: First line: 0"
- Formatted: Font: Italic
- Formatted: Font: Italic

572 We demonstrated that both temperature and non-thermal processes exert control
573 on $p\text{CO}_2$, but non-thermal control generally surpasses thermal control in ASC over
574 multiple time scales (Fig. 6, Table S4, T/B<1). The magnitude of $p\text{CO}_2$ variation
575 attributed to non-thermal processes varied greatly (i.e., $\Delta p\text{CO}_{2,\text{nt}}$ had large standard
576 deviations, Table S4). For example, during the year of strongest non-thermal control
577 (2016), $\Delta p\text{CO}_{2,\text{nt}}$ was 534 μatm versus $\Delta p\text{CO}_{2,\text{nt}}$ of 209 μatm in the year of weakest
578 thermal control (2019). Conversely, the magnitude of $p\text{CO}_2$ variation attributed to
579 temperature was consistent across time scales. For example, during the year of strongest
580 thermal control (2015), $\Delta p\text{CO}_{2,\text{t}}$ was 276 μatm versus $\Delta p\text{CO}_{2,\text{t}}$ of 242 μatm in the year of
581 weakest thermal control (2017). Spring and fall seasons, which experienced the greatest
582 temperature swings (Table S1), had greater relative temperature control exerted on $p\text{CO}_2$
583 out of all seasons (Fig. 6, Table S4). The difference in T/B between sampling methods is
584 relatively small over the 10-month sensor deployment period, but it is worth noting that
585 T/B did not align over shorter seasonal time scales sampling methods (Fig. 6, Table S4).
586 Continuous monitoring demonstrated a greater magnitude of fluctuation resulting from
587 both temperature and non-thermal processes (i.e., greater $\Delta p\text{CO}_{2,\text{t}}$ and $\Delta p\text{CO}_{2,\text{nt}}$),
588 indicating that the extremes are generally not captured by the discrete, daytime sampling,
589 and sensor data would provide a better understanding of system controls.

590 The greater influence of non-thermal controls that we report conflicts with Yao
591 and Hu (2017), who found that ASC was primarily thermally controlled (T/B 1.53 – 1.79)
592 from May 2014 to April 2015. Yao and Hu (2017) also found that locations in the upper
593 estuary experienced lower T/B during flooding conditions than drought conditions.
594 Although the opposite was found at ASC, it is likely that the high T/B calculated at ASC

595 by Yao and Hu (2017) was still a result of the drought condition due to the long residence
596 time of the estuary. Since 2015, there has not been another significant drought in the
597 system, so it seems that non-thermal controls on $p\text{CO}_2$ are more important at this location
598 under normal freshwater inflow conditions.

599 Significantly warmer water temperatures were observed during the nighttime in
600 both summer and fall (Fig. 5), indicating that temperature could exert a slight control on
601 the carbonate system over a diel time scale. We note that significant differences in day
602 and night temperature within seasons do not indicate that diel differences were observed
603 on all days within the season, as large standard deviations in both daytime and nighttime
604 values result in considerable overlap. More substantial temperature swings between
605 seasons would result in more temperature control over a seasonal timescale. ASC seems
606 to have less thermal control of the carbonate system than offshore GOM waters, as
607 temperature had substantially higher explanatory value for pH and $p\text{CO}_2$ based on simple
608 linear regressions in offshore GOM waters ($R^2 = 0.81$ and 0.78, respectively (Hu et al.,
609 2018)) than at ASC ($R^2 = 0.30$ and 0.52, respectively, for sensor data and $R^2 = 0.38$ and
610 0.25, respectively, for discrete data)).

611 Though annual average $p\text{CO}_2$ (and CO_2 flux) are higher in the upper MAE and
612 lower offshore than at our study site, the same seasonal patterns that we observed (i.e.,
613 elevated $p\text{CO}_2$ and positive CO_2 flux in the summer and depressed $p\text{CO}_2$ and negative
614 CO_2 flux during the winter, Table S1, Fig. S1) has also been observed throughout the
615 entire MAE and the open Gulf of Mexico (Hu et al., 2018; Yao and Hu, 2017). These
616 seasonal patterns correspond with both the directional response of the system to
617 temperature and net community metabolism response to changing temperature, i.e.,

618 elevated respiration in summer months (Caffrey, 2004). Despite that there were no
619 observations of hypoxia, there was a strong relationship between the carbonate system
620 parameters and DO (Fig. 7, Table S5), suggesting that net ecosystem metabolism may
621 exert an important control on the carbonate system on ~~certain seasonal~~ time scales. The
622 lack of day-night difference in DO (Fig. 5F) despite the significant day-night difference
623 in both pH and $p\text{CO}_2$ suggests that net community metabolism is likely not a strong
624 controlling factor on diel time scales. Biological control likely becomes more important
625 over seasonal timescales.

626 *4.2.2 Tidal control on carbonate chemistry*

627 While the tidal range in the northwestern GOM is relatively small (1.30 m over
628 our 10-month continuous monitoring period), the tidal inlet location of our study site
629 results in proportionally more “coastal water” during high tide and proportionally more
630 “estuarine water” during low tide. The carbonate chemistry signal of these different water
631 masses was seen in the differences between high tide and low tide conditions at ASC
632 (i.e., high tide having lower $p\text{CO}_2$ because coastal waters are less heterotrophic than
633 estuarine waters, Table 2). Consequently, the relative importance of thermal versus non-
634 thermal controls may be modulated by tide level. We calculated the thermal and non-
635 thermal $p\text{CO}_2$ terms separately during high tide and low tide periods and found that non-
636 thermal control is more important during low tide conditions (within each season T/B is
637 0.10 ± 0.07 lower during the low tide than high tide). This is likely because low tide has
638 proportionally more “estuarine water” at the location and because there is less volume of
639 water for the end products of biological processes to accumulate. The difference in T/B

Formatted: Font: Italic

Formatted: Indent: First line: 0"

Formatted: Font: Italic

640 between high tide and low tide conditions was greatest in the spring, likely due to a
641 combination of elevated spring-time productivity and larger tidal ranges in the spring.

642 The GOM is one of the few places in the world that experiences diurnal tides
643 (Seim et al., 1987; Thurman, 1994), so theoretically, the fluctuations in $p\text{CO}_2$ associated
644 with tides may align to either amplify or reduce/reverse the fluctuations that would result
645 from diel variability in net community metabolism. Based on diel tidal fluctuations at this
646 site (i.e., higher tides during the day in the spring and summer and higher tides at night
647 during the winter, Fig. 5E) and the higher $p\text{CO}_2$ associated with low tide (Table 2), tidal
648 control should amplify the biological signal (nighttime $p\text{CO}_2 >$ daytime $p\text{CO}_2$) during
649 spring and summer and reduce or reverse the biological signal during the winter. This
650 tidal control can explain the diel variability present in our $p\text{CO}_2$ data, which showed the
651 full reversal of the expected biological signal in the winter (Fig. 5C, Table S3, nighttime
652 $p\text{CO}_2 <$ daytime $p\text{CO}_2$), i.e., the higher nighttime tides in winter brought in enough low
653 CO_2 water from offshore to fully offset any nighttime buildup of CO_2 from the lack of
654 photosynthesis. However, we note that the expected diel, biological control was likely
655 minimal since daytime DO was not consistently higher than nighttime DO (Fig. 5F). The
656 same seasonal pattern diel tide fluctuations were exhibited from Dec 20, 2016 (when the
657 tide data is first available) through the rest of our discrete monitoring period (Feb 25,
658 2020), indicating that tidal control on diel variability of carbonate system parameters was
659 likely consistent throughout this 3+ year period. The diel variability in pH did not mirror
660 $p\text{CO}_2$ as would be expected (Fig. 5). The relationship between pH and tide level more
661 closely mirrored the relationships of salinity and temperature with tide level (versus $p\text{CO}_2$

662 relationship with tide level; Table 2), indicating that controlling factors of the carbonate
663 system may not be exerted equally on both pH and $p\text{CO}_2$ over different time scales.

664 *4.2.3 Salinity and freshwater inflow controls on carbonate chemistry*

665 Previous studies have indicated that freshwater inflow may exert a primary
666 control on the carbonate system in the estuaries of the northwestern GOM (Hu et al.,
667 2015; Yao et al., 2020; Yao and Hu, 2017). Carbonate system variability is much lower at
668 ASC than it is in the more upper reaches of MAE, likely due to the lesser influence of
669 freshwater inflow and its associated changes in biological activity at ASC (Yao and Hu,
670 2017). Given the location of our sampling in the lower portion of the estuary and the
671 long residence time in the system, we did not directly address river discharge as a
672 controlling factor, but the influence of freshwater inflow may be evident in the response
673 of the system to changes in salinity. Fluctuating salinity at ASC may also result from
674 direct precipitation, stratification, and tidal fluctuations; however, the low R^2 (0.02)
675 associated with a simple linear regression between tide level and salinity ($p < 0.0001$)
676 indicates that salinity fluctuations are more indicative of non-tidal factors. Salinity data
677 from both sensor and discrete monitoring were strongly correlated with both pH and
678 $p\text{CO}_2$, with correlation coefficients nearing (continuous) or surpassing (discrete) that of
679 the correlations with temperature (Fig. 7; Table S5). **Periods of lower salinity had higher**
680 **pH and lower $p\text{CO}_2$, likely due to enhanced freshwater influence and subsequent elevated**
681 **primary productivity at the study site.**

682 *4.2.4 Windspeed and CO_2 inventory*

683 We investigated wind speed as a possible control on the carbonate system to gain
684 insight into the effect of wind-driven CO_2 fluxes on the inventory of CO_2 in the water

Formatted: Font: Italic

Formatted: Indent: First line: 0"

Formatted: Font: Italic

Formatted: Indent: First line: 0"

Formatted: Font: Italic, Subscript

Formatted: Font: Italic

685 column (and subsequent impacts to the entire carbonate system). The Texas coast has
686 relatively high wind speeds, with the mean wind speed observed during our continuous
687 monitoring period being 5.8 m s^{-1} . While this results in relatively high calculated CO_2
688 fluxes (Fig. 3), the seasonal relationship between $p\text{CO}_2$ and windspeed does not support a
689 change in inventory with higher winds. Since spring and summer both have a mean
690 estuarine $p\text{CO}_2$ greater than atmospheric level (and positive CO_2 flux, Table S1) a
691 negative relationship between windspeed and $p\text{CO}_2$ would be necessary to support this
692 hypothesis, but winter, spring, and fall all experience increases in $p\text{CO}_2$ with increasing
693 wind based on simple linear regression.

694 *4.3 Carbonate chemistry as a component of overall system variability*

695 Estuaries and coastal areas are dynamic systems with human influence, riverine
696 influence, and influence from an array of biogeochemical processes, resulting in highly
697 variable environmental conditions. Based on an LDA used to assess overall system
698 variability using a suite of environmental parameters compiled at a single location, we
699 can conclude that carbonate chemistry parameters are among the most important of
700 variants on both daily and seasonal time scales in this coastal setting. Of the two
701 carbonate system components that we incorporated (pH and $p\text{CO}_2$), $p\text{CO}_2$ was the most
702 critical in discriminating along diel or seasonal scales despite similar seasonal differences
703 that were identified by ANOVA (Table S2) and more seasons with significant diel
704 differences in pH (Table S3). pH seemed to be a larger component of overall system
705 variability on a seasonal time scale (compared to the very small contribution seen on a
706 diel scale, Table 1). Given that the seasonal and diel variability in carbonate chemistry at
707 this location is relatively small compared to other coastal areas that are in the literature,

708 the high contribution of carbonate chemistry to overall system variability that we detected
709 is likely to be present at other coastal locations around the world.

710 **5. Conclusions**

711 We monitored carbonate chemistry parameters (pH and $p\text{CO}_2$) using both sensor
712 deployments (10 months) and discrete sample collection (5+ years) at the Aransas Ship
713 Channel, TX, to characterize temporal variability. Significant seasonal variability and
714 diel variability in carbonate system parameters were both present at the location. Diel
715 fluctuations were smaller than many other areas previously studied. The difference
716 between daytime and nighttime values of carbonate system parameters varied between
717 seasons, occasionally reversing the expected diel variability due to biological processes.
718 Tide level (despite the small tidal range), temperature, freshwater influence, and
719 biological activity all seem to exert important controls on the carbonate system at the
720 location. The relative importance of the different controls varied with timescale, and
721 controls were not always exerted equally on both pH and $p\text{CO}_2$. Carbonate chemistry
722 (particularly $p\text{CO}_2$) was among the most important environmental parameters to in
723 overall system variability to distinguish between both diel and seasonal environmental
724 conditions.

725 Despite known temporal variability on shorter timescales, discrete sampling was
726 generally representative of the average carbonate system on a seasonal and annual basis
727 based on comparison with our sensor data. Discrete data captured interannual variability,
728 which could not be captured by the shorter-term continuous sensor data. Additionally,
729 there was no difference in CO_2 flux between sampling types. All of these findings

730 supporting the validity of discrete sample collection for carbonate system characterization
731 at this location.

732 This is one of the first studies that ~~investigates~~ high-temporal frequency data from
733 deployed sensors that measure carbonate system parameters in an estuary-influenced
734 environment. Long-term, effective deployments of these monitoring tools could greatly
735 improve our understanding of estuarine systems. This study's detailed investigation of
736 data from multiple, co-located environmental sensors was able to provide insight into
737 potential driving forces of carbonate chemistry on diel and seasonal time scales; this
738 provides strong support for the implementation of carbonate chemistry monitoring in
739 conjunction with preexisting coastal environmental monitoring infrastructure.

740 Strategically locating such sensors in areas that are subject to local acidification drivers
741 or support large biodiversity or commercially important species may be the most crucial
742 in guiding future mitigation and adaptation strategies for natural systems and aquaculture
743 facilities.

744

745 **Data availability**

746 Continuous sensor data are archived with the National Oceanic and Atmospheric
747 Administration's (NOAA's) National Centers for Environmental Information (NCEI)
748 (<https://doi.org/10.25921/dkg3-1989>). Discrete sample data are available in two separate
749 datasets archived with National Science Foundation's Biological & Chemical
750 Oceanography Data Management Office (BCO-DMO) (doi:10.1575/1912/bco-
751 dmo.784673.1 and doi: 10.26008/1912/bco-dmo.835227.1).

752 **Author Contribution**

753 MM and XH defined the scope of this work. XH received funding for all components of
754 the work. MM, HY, and CJS performed field sampling and laboratory analysis of
755 samples. MM prepared the initial manuscript and all co-authors contributed to revisions.

756 **Competing interests**

757 The authors declare that they have no conflict of interest.

758

759 **Acknowledgements**

760 Funding for autonomous sensors and sensor deployment was provided by the
761 United States Environmental Protection Agency's National Estuary Program via the
762 Coastal Bend Bays and Estuaries Program Contract No. 1605. Thanks to Rae Mooney
763 from Coastal Bend Bays and Estuaries Program for assistance in the initial sensor setup.
764 Funding for discrete sampling as well MM's dissertation research has been supported by
765 both NOAA National Center for Coastal Ocean Science (Contract No.
766 NA15NOS4780185) and NSF Chemical Oceanography Program (OCE-1654232). We
767 also appreciate the support from the Mission-Aransas National Estuarine Research
768 Reserve in allowing us the boat-of-opportunity for our ongoing discrete sample
769 collections and the University of Texas Marine Science Institute for allowing us access to
770 their research pier for the sensor deployment. A special thanks to Hongjie Wang, Lisette
771 Alcocer, Allen Dees, and Karen Alvarado for assistance with field work. We would also
772 like to thank Melissa Ward, our other anonymous referee, and the Associate Editor, Tyler
773 Cyronak, for aiding in the considerable improvement of this manuscript.

774 **References**

775 Barton, A., Waldbusser, G.G., Feely, R.A., Weisberg, S.B., Newton, J.A., Hales, B.,
776 Cudd, S., Eudeline, B., Langdon, C.J., Jefferds, I., King, T., Suurbier, A.,
777 McLaughlin, K., 2015. Impacts of coastal acidification on the pacific northwest
778 shellfish industry and adaptation strategies implemented in response. *Oceanography*
779 28, 146–159.

780 Bednaršek, N., Tarling, G.A., Bakker, D.C.E., Fielding, S., Jones, E.M., Venables, H.J.,
781 Ward, P., Kuzirian, A., Lézé, B., Feely, R.A., Murphy, E.J., 2012. Extensive
782 dissolution of live pteropods in the Southern Ocean. *Nat. Geosci.* 5, 881–885.
783 <https://doi.org/10.1038/ngeo1635>

784 Borges, A. V., 2005. Do we have enough pieces of the jigsaw to integrate CO₂ fluxes in
785 the coastal ocean ? *Estuaries* 28, 3–27.

786 Borges, A. V., Abril, G., 2011. Carbon Dioxide and Methane Dynamics in Estuaries,
787 Treatise on Estuarine and Coastal Science. <https://doi.org/10.1016/B978-0-12-374711-2.00504-0>

789 Bresnahan, P.J., Martz, T.R., Takeshita, Y., Johnson, K.S., LaShomb, M., 2014. Best
790 practices for autonomous measurement of seawater pH with the Honeywell Durafet.
791 *Methods Oceanogr.* 9, 44–60. <https://doi.org/10.1016/j.mio.2014.08.003>

792 Caffrey, J.M., 2004. Factors controlling net ecosystem metabolism in U.S. estuaries.
793 *Estuaries* 27, 90–101. <https://doi.org/10.1007/BF02803563>

794 Cai, W.-J., 2011. Estuarine and Coastal Ocean Carbon Paradox: CO₂ Sinks or Sites of
795 Terrestrial Carbon Incineration? *Ann. Rev. Mar. Sci.* 3, 123–145.
796 <https://doi.org/10.1146/annurev-marine-120709-142723>

Formatted: Subscript

Formatted: Subscript

797 Cai, W.-J., Hu, X., Huang, W.-J., Murrell, M.C., Lehrter, J.C., Lohrenz, S.E., Chou, W.-
798 C., Zhai, W., Hollibaugh, J.T., Wang, Y., Zhao, P., Guo, X., Gundersen, K., Dai, M.,
799 Gong, G.-C., 2011. Acidification of subsurface coastal waters enhanced by
800 eutrophication. *Nat. Geosci.* 4, 766–770. <https://doi.org/10.1038/ngeo1297>
801 Challener, R.C., Robbins, L.L., Mcclintock, J.B., 2016. Variability of the carbonate
802 chemistry in a shallow, seagrass-dominated ecosystem: Implications for ocean
803 acidification experiments. *Mar. Freshw. Res.* 67, 163–172.
804 <https://doi.org/10.1071/MF14219>
805 Crosswell, J.R., Anderson, I.C., Stanhope, J.W., Van Dam, B., Brush, M.J., Ensign, S.,
806 Piehler, M.F., McKee, B., Bost, M., Paerl, H.W., 2017. Carbon budget of a shallow,
807 lagoonal estuary: Transformations and source-sink dynamics along the river-estuary-
808 ocean continuum. *Limnol. Oceanogr.* 62, S29–S45.
809 <https://doi.org/10.1002/lno.10631>
810 Cyronak, T., Andersson, A.J., D'Angelo, S., Bresnahan, P., Davidson, C., Griffin, A.,
811 Kindeberg, T., Pennise, J., Takeshita, Y., White, M., 2018. Short-term spatial and
812 temporal carbonate chemistry variability in two contrasting seagrass meadows:
813 Implications for pH buffering capacities. *Estuaries and Coasts* 41, 1282–1296.
814 <https://doi.org/10.1007/s12237-017-0356-5>
815 Dickson, A.G., 1990. Standard potential of the reaction: $\text{AgCl}(\text{s}) + 1/2\text{H}_2(\text{g}) = \text{Ag}(\text{s}) + \text{HCl}(\text{aq})$, and the standard acidity constant of the ion HSO_4^- in synthetic sea
816 water from 273.15 to 318.15 K. *J. Chem. Thermodyn.* 22, 113–127.
817 [https://doi.org/10.1016/0021-9614\(90\)90074-Z](https://doi.org/10.1016/0021-9614(90)90074-Z)
818 Ekstrom, J. a., Suatoni, L., Cooley, S.R., Pendleton, L.H., Waldbusser, G.G., Cinner, J.E.,

Formatted: Subscript

820 Ritter, J., Langdon, C., van Hoidonk, R., Gledhill, D., Wellman, K., Beck, M.W.,
821 Brander, L.M., Rittschof, D., Doherty, C., Edwards, P.E.T., Portela, R., 2015.
822 Vulnerability and adaptation of US shellfisheries to ocean acidification. *Nat. Clim.*
823 *Chang.* 5, 207–214. <https://doi.org/10.1038/nclimate2508>

824 Gazeau, F., Quiblier, C., Jansen, J.M., Gattuso, J.-P., Middelburg, J.J., Heip, C.H.R.,
825 2007. Impact of elevated CO₂ on shellfish calcification. *Geophys. Res. Lett.* 34, Formatted: Subscript
826 L07603. <https://doi.org/10.1029/2006GL028554>

827 Gobler, C.J., Talmage, S.C., 2014. Physiological response and resilience of early life-
828 stage Eastern oysters (*Crassostrea virginica*) to past, present and future ocean Formatted: Font: Italic
829 acidification. *Conserv. Physiol.* 2, 1–15.
830 <https://doi.org/10.1093/conphys/cou004.Introduction>

831 Ho, D.T., Law, C.S., Smith, M.J., Schlosser, P., Harvey, M., Hill, P., 2006.
832 Measurements of air-sea gas exchange at high wind speeds in the Southern Ocean:
833 Implications for global parameterizations. *Geophys. Res. Lett.* 33, 1–6.
834 <https://doi.org/10.1029/2006GL026817>

835 Hofmann, G.E., Smith, J.E., Johnson, K.S., Send, U., Levin, L. a, Micheli, F., Paytan, A.,
836 Price, N.N., Peterson, B., Takeshita, Y., Matson, P.G., Crook, E.D., Kroeker, K.J.,
837 Gambi, M.C., Rivest, E.B., Frieder, C. a, Yu, P.C., Martz, T.R., 2011. High-
838 frequency dynamics of ocean pH: a multi-ecosystem comparison. *PLoS One* 6,
839 e28983. <https://doi.org/10.1371/journal.pone.0028983>

840 Hsu S. A., 1994. Determining the power-law wind-profile exponent under near-neatral
841 stability condiditions at sea. *J. Appl. Meteorol.* 33, 757–765.

842 Hu, X., Beseres Pollack, J., McCutcheon, M.R., Montagna, P. a., Ouyang, Z., 2015.

843 Long-term alkalinity decrease and acidification of estuaries in Northwestern Gulf of
844 Mexico. Environ. Sci. Technol. 49, 3401–3409. <https://doi.org/10.1021/es505945p>

845 Hu, X., Nuttall, M.F., Wang, H., Yao, H., Staryk, C.J., McCutcheon, M.R., Eckert, R.J.,
846 Embesi, J.A., Johnston, M.A., Hickerson, E.L., Schmahl, G.P., Manzello, D.,
847 Enochs, I.C., DiMarco, S., Barbero, L., 2018. Seasonal variability of carbonate
848 chemistry and decadal changes in waters of a marine sanctuary in the Northwestern
849 Gulf of Mexico. Mar. Chem. 205, 16–28.
850 <https://doi.org/10.1016/j.marchem.2018.07.006>

851 Jiang, L.-Q., Cai, W.-J., Wang, Y., 2008. A comparative study of carbon dioxide
852 degassing in river- and marine-dominated estuaries. Limnol. Oceanogr. 53, 2603–
853 2615. <https://doi.org/10.4319/lo.2008.53.6.2603>

854 Jiang, L.Q., Cai, W.J., Wang, Y., Bauer, J.E., 2013. Influence of terrestrial inputs on
855 continental shelf carbon dioxide. Biogeosciences 10, 839–849.
856 <https://doi.org/10.5194/bg-10-839-2013>

857 Kealoha, A.K., Shamberger, K.E.F., DiMarco, S.F., Thyng, K.M., Hetland, R.D.,
858 Manzello, D.P., Slowey, N.C., Enochs, I.C., 2020. Surface water CO_2 variability in
859 the Gulf of Mexico (1996–2017). Sci. Rep. 10, 1–13.
860 <https://doi.org/10.1038/s41598-020-68924-0>

861 Laruelle, G.G., Cai, W.-J., Hu, X., Gruber, N., Mackenzie, F.T., Regnier, P., 2018.
862 Continental shelves as a variable but increasing global sink for atmospheric carbon
863 dioxide. Nat. Commun. 9, 454. <https://doi.org/10.1038/s41467-017-02738-z>

864 Li, D., Chen, J., Ni, X., Wang, K., Zeng, D., Wang, B., Jin, H., Huang, D., Cai, W.J.,
865 2018. Effects of biological production and vertical mixing on sea surface $p\text{CO}_2$

Formatted: Subscript

Formatted: Font: Italic

Formatted: Subscript

866 variations in the Changjiang River Plume during early autumn: A buoy-based time
867 series study. *J. Geophys. Res. Ocean.* 123, 6156–6173.

868 <https://doi.org/10.1029/2017JC013740>

869 Liu, H., Zhang, Q., Katul, G.G., Cole, J.J., Chapin, F.S., MacIntyre, S., 2016. Large CO₂
870 effluxes at night and during synoptic weather events significantly contribute to CO₂
871 emissions from a reservoir. *Environ. Res. Lett.* 11, 1–8.

872 <https://doi.org/10.1088/1748-9326/11/6/064001>

873 Mathis, J.T., Pickart, R.S., Byrne, R.H., Mcneil, C.L., Moore, G.W.K., Juranek, L.W.,
874 Liu, X., Ma, J., Easley, R.A., Elliot, M.M., Cross, J.N., Reisdorph, S.C., Bahr, F.,
875 Morison, J., Lichendorf, T., Feely, R.A., 2012. Storm-induced upwelling of high *p*
876 CO₂ waters onto the continental shelf of the western Arctic Ocean and implications
877 for carbonate mineral saturation states. *Geophys. Res. Lett.* 39, 4–9.

878 <https://doi.org/10.1029/2012GL051574>

879 McCutcheon, M.R., Staryk, C.J., Hu, X., 2019. Characteristics of the carbonate system in
880 a semiarid estuary that experiences summertime hypoxia. *Estuaries and Coasts* 42,
881 1509–1523. <https://doi.org/10.1007/s12237-019-00588-0>

882 Millero, F.J., 2010. Carbonate constant for estuarine waters. *Mar. Freshw. Res.* 61, 139–
883 142.

884 Montagna, P.A., Brenner, J., Gibeaut, J., Morehead, S., 2011. Chapter 4: Coastal Impacts,
885 in: Jurgen Schmandt, Gerald R. North, and J.C. (Ed.), *The Impact of Global
886 Warming on Texas*. University of Texas Press, pp. 96–123.

887 Raymond, P.A., Cole, J.J., 2001. Gas exchange in rivers and estuaries: Choosing a gas
888 transfer velocity. *Estuaries* 24, 312–317. <https://doi.org/10.2307/1352954>

889 Robbins, L.L., Lisle, J.T., 2018. Regional acidification trends in florida shellfish
890 estuaries: a 20+ year look at pH, oxygen, temperature, and salinity. *Estuaries and*
891 *Coasts* 41, 1268–1281. <https://doi.org/10.1007/s12237-017-0353-8>

892 Sastri, A.R., Christian, J.R., Achterberg, E.P., Atamanchuk, D., Buck, J.J.H., Bresnahan,
893 P., Duke, P.J., Evans, W., Gonski, S.F., Johnson, B., Juniper, S.K., Mihaly, S.,
894 Miller, L.A., Morley, M., Murphy, D., Nakaoka, S.I., Ono, T., Parker, G., Simpson,
895 K., Tsunoda, T., 2019. Perspectives on in situ sensors for ocean acidification
896 research. *Front. Mar. Sci.* 6, 1–6. <https://doi.org/10.3389/fmars.2019.00653>

897 Schulz, K.G., Riebesell, U., 2013. Diurnal changes in seawater carbonate chemistry
898 speciation at increasing atmospheric carbon dioxide. *Mar. Biol.* 160, 1889–1899.
899 <https://doi.org/10.1007/s00227-012-1965-y>

900 Seim, H.E., Kjerfve, B., Snead, J.E., 1987. Tides of Mississippi Sound and the adjacent
901 continental shelf. *Estuar. Coast. Shelf Sci.* 25, 143–156.
902 [https://doi.org/10.1016/0272-7714\(87\)90118-1](https://doi.org/10.1016/0272-7714(87)90118-1)

903 Semesi, I.S., Beer, S., Björk, M., 2009. Seagrass photosynthesis controls rates of
904 calcification and photosynthesis of calcareous macroalgae in a tropical seagrass
905 meadow. *Mar. Ecol. Prog. Ser.* 382, 41–47. <https://doi.org/10.3354/meps07973>

906 Solis, R.S., Powell, G.L., 1999. Hydrography, Mixing Characteristics, and Residence
907 Time of Gulf of Mexico Estuaries, in: Bianchi, T.S., Pennock, J.R., Twilley, R.R.
908 (Eds.), *Biogeochemistry of Gulf of Mexico Estuaries*. John Wiley & Sons, Inc: New
909 York, pp. 29–61.

910 Takahashi, T., Sutherland, S.C., Sweeney, C., Poisson, A., Metzl, N., Tilbrook, B., Bates,
911 N., Wanninkhof, R., Feely, R.A., Sabine, C., Olafsson, J., Nojiri, Y., 2002. Global

912 sea-air CO₂ flux based on climatological surface ocean *p*CO₂, and seasonal
913 biological and temperature effects. Deep. Res. Part II Top. Stud. Oceanogr. 49,
914 1601–1622. [https://doi.org/10.1016/S0967-0645\(02\)00003-6](https://doi.org/10.1016/S0967-0645(02)00003-6)

915 Thurman, H. V., 1994. Introductory Oceanography, Seventh Edition. pp. 252–276.

916 Uppström, L.R., 1974. The boron/chlorinity ratio of deep-sea water from the Pacific
917 Ocean. Deep. Res. Oceanogr. Abstr. 21, 161–162. [https://doi.org/10.1016/0011-7471\(74\)90074-6](https://doi.org/10.1016/0011-7471(74)90074-6)

919 USGS, 2001. Discharge Between San Antonio Bay and Aransas Bay, Southern Gulf
920 Coast, Texas, May-September 1999.

921 Van Dam, B.R., Edson, J.B., Tobias, C., 2019. Parameterizing Air-Water Gas Exchange
922 in the Shallow, Microtidal New River Estuary. J. Geophys. Res. Biogeosciences
923 124, 2351–2363. <https://doi.org/10.1029/2018JG004908>

924 Waldbusser, G.G., Salisbury, J.E., 2014. Ocean acidification in the coastal zone from an
925 organism's perspective: multiple system parameters, frequency domains, and
926 habitats. Ann. Rev. Mar. Sci. 6, 221–47. <https://doi.org/10.1146/annurev-marine-121211-172238>

928 Wanninkhof, R., 1992. Relationship between wind speed and gas exchange. J. Geophys.
929 Res. 97, 7373–7382. <https://doi.org/10.1029/92JC00188>

930 Wanninkhof, R., Asher, W.E., Ho, D.T., Sweeney, C., McGillis, W.R., 2009. Advances
931 in quantifying air-sea gas exchange and environmental forcing. Ann. Rev. Mar. Sci.
932 1, 213–244. <https://doi.org/10.1146/annurev.marine.010908.163742>

933 Weiss, R.F., 1974. Carbon dioxide in water and seawater: the solubility of a non-ideal
934 gas. Mar. Chem. 2, 203–215.

Formatted: Subscript

Formatted: Font: Italic

Formatted: Subscript

935 Westfall, P.H., 1997. Multiple testing of general contrasts using logical constraints and
936 correlations. *J. Am. Stat. Assoc.* 92, 299–306.

937 <https://doi.org/10.1080/01621459.1997.10473627>

938 Yao, H., Hu, X., 2017. Responses of carbonate system and CO₂ flux to extended drought
939 and intense flooding in a semiarid subtropical estuary. *Limnol. Oceanogr.* 62, S112–
940 S130. <https://doi.org/10.1002/lno.10646>

Formatted: Subscript

941 Yao, H., McCutcheon, M.R., Staryk, C.J., Hu, X., 2020. Hydrologic controls on CO₂
942 chemistry and flux in subtropical lagoonal estuaries of the northwestern Gulf of
943 Mexico. *Limnol. Oceanogr.* 65, 1380–1398. <https://doi.org/10.1002/lno.11394>

944 Yates, K.K., Dufore, C., Smiley, N., Jackson, C., Halley, R.B., 2007. Diurnal variation of
945 oxygen and carbonate system parameters in Tampa Bay and Florida Bay. *Mar.*
946 *Chem.* 104, 110–124. <https://doi.org/10.1016/j.marchem.2006.12.008>

Formatted: Subscript

947